Sensors and Actuators B 145 (2010) 769–774

Contents lists available at ScienceDirect

Sensors and Actuators B: Chemical

journal homepage: www.elsevier.com/locate/snb

Optical and physical characterization of a local evanescent array coupled biosensor: Use of evanescent field perturbations for multianalyte sensing

Matthew D. Stephens[b], Guangwei Yuan[a], Kevin L. Lear[a], David S. Dandy[b,*]

[a] Dept. of Electrical and Computer Engineering, Colorado State University, Fort Collins, CO, USA
[b] Dept. of Chemical and Biological Engineering, Colorado State University, 1370 Campus Delivery, Fort Collins, CO 80523, USA

ARTICLE INFO

Article history:
Received 18 August 2009
Received in revised form 18 January 2010
Accepted 20 January 2010
Available online 1 February 2010

Keywords:
Evanescent field
Waveguide
Biosensor
NSOM

ABSTRACT

The evanescent field surrounding the core of an optical waveguide is very sensitive to refractive index changes near the core. This sensitivity can be exploited to form the basis for a quantitative sensor with high specificity and sensitivity. Selective probe molecules may be attached to the surface of a waveguide core and the evanescent field locally monitored as target analytes are introduced to the system. In this study, probe/analyte regions were simulated using lithographically patterned organic films with thicknesses of 60 nm and 130 nm. The evanescent field strength was measured quantitatively using near field scanning optical microscopy (NSOM). The presence of the organic material on the waveguide caused up to a 70% change in the intensity of the evanescent field over the patterned region and the excitation of a weakly bound higher order mode. The waveguide core and surrounding cladding were numerically simulated using the beam propagation method and these predictions are in quantitative agreement with the experimental results obtained using NSOM.

1. Introduction

The need for a rapid, multianalyte, quantitative sensor for the detection of biological or environmental analytes has long been established [1–4]. There have been many examples of analytical devices that use antibody/antigen binding as a method of sensing and sandwich assays that use fluorescently labeled antibodies have been a laboratory standard [1–6]. But the addition of labeled antibodies adds an additional step to the diagnostic process, and limits the multianalyte capability of the test. If an available method were capable of directly and locally detecting the probe/analyte interaction itself, this would make the diagnostic method more applicable to real-world problems.

A waveguide is able to carry light down its length by confining the energy to a central region called the core. The light is confined by means of a refractive index difference between the core of the waveguide and the surrounding regions, referred to as the cladding. But not all of the guided optical power is carried in the core region. A fraction of the power is carried in the lower refractive index materials surrounding the waveguide core. This portion of light that is carried outside the core is the evanescent field. It has been observed that the thinner the core region, the farther the evanescent field will extend away from the core and into the cladding. This means that, for a relatively thin core region, the evanescent field is able to interact with the cladding layers up to hundreds of nanometers from the core [7–10]. The equations describing evanescent field penetration into the optical cladding predict that the field can shift its power distribution spatially in response to changes in the refractive index in the cladding regions. This shift in field forms the basis for detecting the binding of target analytes to probe molecules that have been immobilized on the surface of the waveguide core.

The sensor operation is based on capturing target analyte out of a sample milieu and allowing the captured analytes to interact with the evanescent field. The most common example of a waveguide is an optical fiber. However, due to the cylindrical nature of a fiber, and the difficulty of manipulating the fiber to effectively expose the evanescent field, a thin-film, planar waveguide is a more favorable geometry. The probe regions are patterned in an array attached directly to the high refractive index core of the waveguide (two probe regions are shown in Fig. 1). When an aqueous mixture is brought into contact with the sensor surface, complementary analytes will diffuse toward the capture regions and bind or hybridize with their respective probes. As the capture events take place, the sample milieu immediately adjacent to the core, assuming water with a refractive index of 1.33, will be displaced by the captured analytes that have a refractive index from 1.35 to 1.6 [13–15]. Binding occurs at the surface of the waveguide core, and as a result the bound analyte becomes part of the optical cladding of the waveguide. By monitoring the evanescent field it is possible to infer that binding is occurring in locations where there is a shift in the field intensity. However, there are a number of important issues to be addressed in this system: (1) the degree to which

* Corresponding author. Tel.: +1 970 491 7437; fax: +1 970 491 7369.
E-mail address: dandy@colostate.edu (D.S. Dandy).

0925-4005/$ – see front matter © 2010 Elsevier B.V. All rights reserved.
doi:10.1016/j.snb.2010.01.046

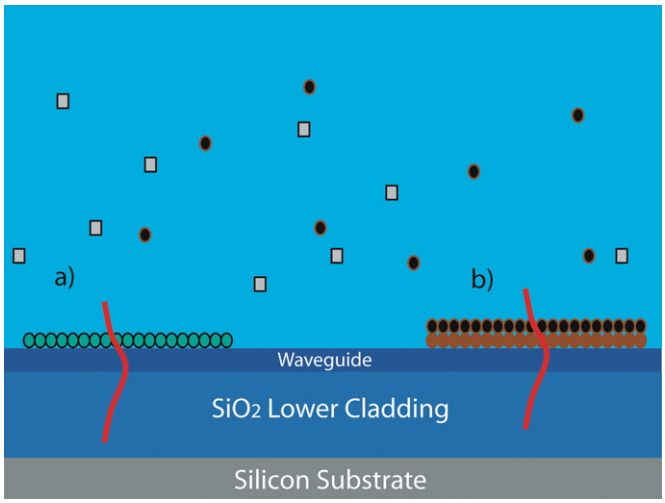

Fig. 1. (a) Evanescent field profile for probe region with no bound analyte. (b) When probes capture analyte from solution, the evanescent field profile shifts up out of the lower cladding.

the evanescent field change depends on the size of the analytes that bind to the surface; (2) the effect of adjacent capture regions on the signal obtained from a region; and (3) the minimum size for a capture region that will provide a detectable change in the evanescent field. To begin to address these issues, the probe/analyte regions have been emulated using well-characterized, precisely defined organic films patterned onto the waveguide surface; these films were selected to have an index similar to that of biological material. A reproducible means of fabricating these regions is via the use of photolithographic techniques. The optical field around these photoresist features was measured using near field scanning optical microscopy (NSOM). The following sections describe how the waveguides were fabricated, the patterning of the photoresist features, the interrogation of the surface evanescent field and the computer simulated response to a representative feature.

2. Materials and methods

2.1. Fabrication of the waveguide

The sensor is based on an asymmetric planar optical waveguide. To fabricate this device an approximately 100 nm thick silicon nitride film was deposited by reactive ion sputtering on a thermally oxidized silicon wafer. The film was deposited using a Nordiko 7000 with a silicon target and NH_3 as the nitrogen source. The deposition pressure for the process was adjusted to deposit in a non-stoichiometric film with a refractive index around 1.8. This sputtering method for film deposition results in an average rms surface roughness of approximately 2 nm. The roughness does have an appreciable impact on the scattering losses from the waveguide and the observed noise in measuring the surface evanescent field intensity. The substrates used to deposit the silicon nitride are thermally oxidized silicon wafers with 2 μm of oxide (Noel Technologies, Campbell, CA). Individual waveguide chips were fabricated from the dielectric coated wafer using conventional photolithography and dry etching techniques. Approximately 1 in. × 1 in. chips were scribed from the wafer and prepared for processing by rinsing in acetone, methanol, and deionized water. After a 120 °C dehydration bake, Microposit S1818 positive photoresist was spun on a chip at 5000–6000 rpm to obtain a 1.8 μm thick layer. Following a 90 °C prebake, the photoresist was exposed using a Karl Suss contact aligner, and the sample was developed and inspected. Ridge waveguides were formed in a Technics MicroRIE plasma etcher in a two step process. An initial etch with O_2 at 50 W was used to descum the sample, then the 15–25 nm waveguide ridges were etched at 50 W using a 4:1 CF_4:O_2 mixture. After stripping the photoresist, clean edges were backside scribed and cleaved perpendicular to the waveguides. Facets on this cleaved edge were polished using a progression of 9 decreasing alumina grit sizes from 30 down to 0.05 μm to allow for end-fire fiber coupling to one of the 2–3 μm wide waveguides. This fabrication process resulted in a TE_{00} single-mode light propagation as confirmed by experimental methods described in Section 2.3 and a simulation package described in Section 2.4.

2.2. Creating the photoresist features on the waveguide

In an earlier study, the effect of core thickness changes on the local evanescent field was explored [11,12]. To more accurately approximate the refractive index profile of an antibody layer with captured antigen or more generally a biological probe layer with captured analyte, photoresist has been used to more closely match the refractive index of biological features. Waveguides have been fabricated as described above and then a thin layer of photoresist (Shipley 1818) with a refractive index of 1.55 was patterned to approximate the refractive index profile and size of attached probe/analyte. To simulate capture of a series of large proteins or virus particles on the waveguide surface, the photoresist thickness was set between 60 nm and 130 nm. To obtain films of this thickness, the stock S1818 photoresist was thinned by the addition of a low viscosity solvent, proplyene glycol monomethyl ether acetate (PGMEA). The thinned photoresist was dispensed on the sample and spun at 5000–6000 rpm to create the film, which was then baked, exposed, and developed using the same procedure as prescribed for the stock S1818. The thickness of the layer of the photoresist was then determined using the topography capabilities of the NSOM. Initially the S1818 was diluted 1:1 by mass with PGMEA, however this resulted in a photoresist coating of approximately 150 nm, which was larger than desired. A solution of 2:1 solvent/photoresist was created and used to coat a wafer at 6000 rpm. This resulted in an approximately 130 nm thick layer of the photoresist. An additional dilution (2.6:1) was produced allowing for the creation of a 60 nm layer of photoresist when spun at 5000 rpm.

2.3. Measuring light response

NSOM was used to interrogate the light field surrounding the waveguide and quantify the impact of the polymer adlayer regions on the evanescent field. In this discussion, the term adlayer is meant to represent the presence of a photolithograpically patterned feature on the surface of the waveguide core. The instrument used to observe the field, an alpha-SNOM (Witec, Ulm, Germany) was placed on an air table and suspended by tension cables to provide a vibration free platform ensuring that topography was measured with reduced environmental noise. The NSOM acquires simultaneous topography and surface evanescent field intensity by raster scanning a cantilever tip across the surface of the sample as described in a previous publication [12]. The tip operates in contact with the surface of the waveguide and collects light from the evanescent field through a 100 nm diameter aperture. This collected light was then amplified with a PMT, and a 3D intensity plot of the local evanescent light field was created. The topography of the sample was determined through deflection of the cantilever tip in contact with the surface. The deflection of the tip was determined by the change in signal from a detector that collects light from a laser beam reflecting off the tip of the cantilever. The cantilever tips were held in place by a magnet and were aligned with the fiber optic cable that collects the light through the tip aperture. The optical path alignment was accomplished by observing

the tip through the instrument's CCD display. The tip was brought in contact with a waveguide and the stage adjusted such that light traveling down the waveguide was observed through the aperture of the tip. The aperture was usually centered over a strong scattering center of the waveguide since this provides a strong signal and light was easily visible through the aperture. The signal from the detector was then monitored as the position of the fiber optic cable was changed using the *x*–*y* positioning knobs. Centering the fiber's location over the aperture maximizes the detected signal, producing the best S/N ratio in the light intensity scans. To quantify the evanescent field intensity, a 100 μm × 100 μm area was scanned while collecting topography and light intensity information. The default settings for the image generation was 256 line scans with 256 data points taken per line scan. The normal scanning speed used was 0.8–1.2 s per line scan in the forward direction and 0.5 s in the reverse direction. If a smaller area was scanned, the number of line scans, scan speed, and data points per line remained the same.

The procedure for measuring the evanescent field strength was as follows: a dc power supply inputted 20–40 mA to a laser diode with an output wavelength of 654 nm. The laser diode was connected to a length of single-mode optical fiber. The fiber provided the light source to end-fire couple light into the waveguide film. The waveguide chip and the associated fiber were bonded onto an aluminum block to provide a stable platform allowing movement of the chip without negatively impacting the coupling alignment. The sample was placed on the stage of the NSOM and the tip brought down into contact with the surface of the waveguide chip. To complete the testing, light/topography scans were taken to determine the evanescent field intensity on the surface of the chip. The data was analyzed using the Image Control image analysis software or exported and plotted with Matlab.

2.4. Modeling field distribution using the beam propagation method

The beam propagation method (BPM) is a mathematical modeling approach that can predict the 2D and 3D propagation of optical energy in a waveguide. Using a commercial BeamPROP software package from RSoft, the 2D optical power distribution was simulated for a waveguide structure with one adlayer feature. The core of the waveguide was simulated with a refractive index of 1.822, the lower cladding layer with 1.45 refractive index, upper cladding with 1.00 refractive index and the feature with 1.55 refractive index. The simulated feature was 8.5 μm long. The incident beam was assumed to be the TE_{00} mode at a wavelength of 654 nm and the thickness of the photoresist layer was 130 nm. The exit boundary condition was set to be a non-reflective boundary. This best approximates the propagation when the waveguide is long enough that reflection from the end of the waveguide is negligible. The transverse and longitudinal grid spacing was 10 nm and 100 nm, respectively. The software package solves the 2D Helmholtz equations that describe field propagation.

3. Results and discussion

Several adlayer sizes and thicknesses were studied to quantify the evanescent field response to the presence of the patterns. Fig. 2 shows an evenly spaced set of 4 photoresist regions fabricated to a thickness of 130 nm. The measured evanescent field over the bare waveguide was observed to have a uniform Gaussian profile, indicating a single bound mode (Fig. 3). This single-mode behavior is optimal for quantification of the response to the presence of an adlayer. Specifically, if the waveguide contains two guided modes, the signal from an adlayer may not be distinguishable from the

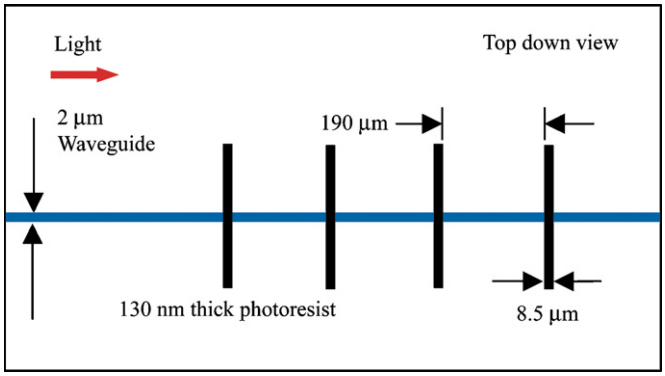

Fig. 2. Mask geometry for fabrication of uniform photoresist features patterned on the waveguide.

oscillation between the modes. As seen in Fig. 4, as light encounters the photoresist feature, there is a drop in the measured surface light intensity followed by a sharp increase at the end of the feature. The lower part of Fig. 4 shows the light intensity measured along the centerline of the 2 μm wide waveguide. The response from the BPM simulations for the 8.5 μm long, 130 nm thick feature is shown in Fig. 5. The centerline scan data shown demonstrates that $\Delta P \sim 70\%$. Here ΔP is defined as the absolute value of the average signal over the pattern less the average power before the pattern divided by the power before the pattern (see Eq. (1)):

$$\Delta P = \left| \frac{Light\_in\_pattern - Light\_before\_pattern}{Light\_before\_pattern} \right| \times 100\% \quad (1)$$

The magnitude of the power modulation must also be compared with the amount of noise present in the signal generated through NSOM scans of the surface evanescent field intensity. The *RMS* (root mean square) noise for a signal is defined as the square root of the absolute value of the sum of variances from the signal (see Eq. (2)). The variance is the expected square deviation of the signal from the average signal. In other words, the *RMS* noise is roughly equivalent to the average difference between a data point and the average signal:

$$RMS = \sqrt{\left| \frac{\sum_{i=1}^{n} \left(X_i - \sum_{i=1}^{n} X_i \right)^2}{n} \right|} \quad (2)$$

where X_i is an individual data point and there are n data points in the signal. The S/N (signal to noise ratio) for a specific response of the evanescent field to a feature is defined as the average difference between the input signal and the signal over the feature divided by

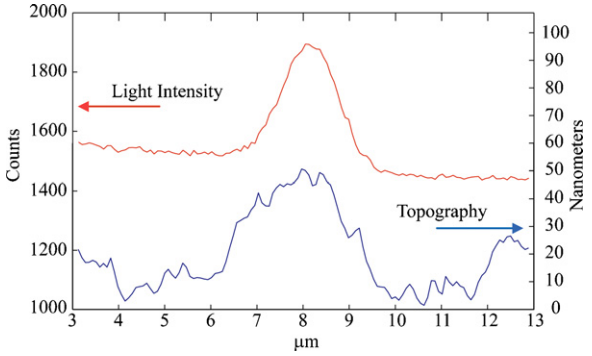

Fig. 3. Cross-section plot of the light intensity (top) and topography (bottom) of an approximately 3 μm wide ridge waveguide etched 14 nm. Light profile indicates a single bound mode.

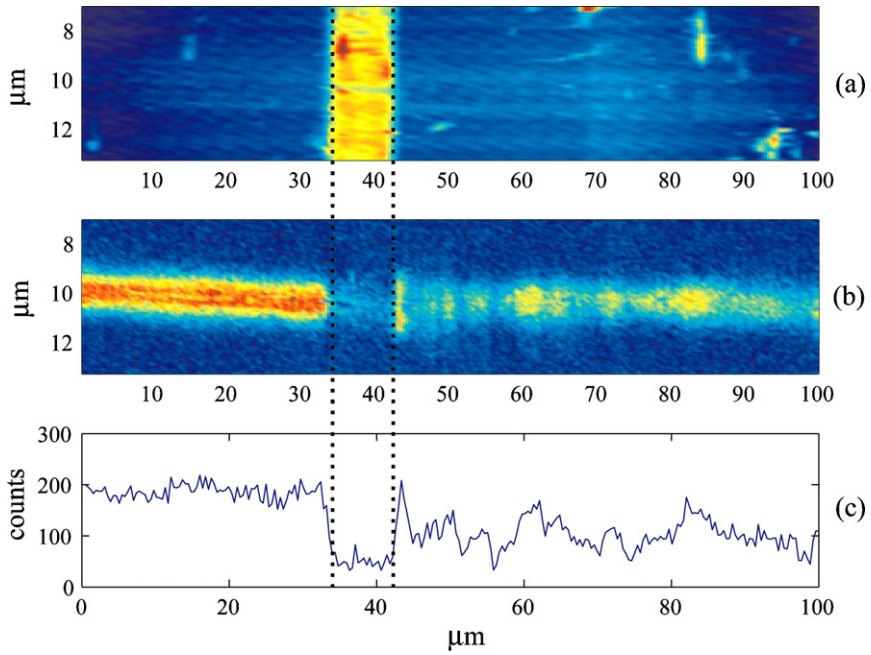

Fig. 4. Experimental light response to the second photoresist features in a series of four. Light propagates from left to right. (a) Topography of 2.0 μm wide waveguide with 14 nm etch depth. Feature size is ≈8.5 μm in length and 130 nm thick, (b) surface light intensity measured with NSOM, and (c) total light measured in photon counts carried in the waveguide after subtracting the background. $\Delta P = 76.9\%$. Dashed lines indicate location of patterned feature.

the *RMS* noise on the input signal (see Eq. (3)):

$$\frac{S}{N} = \frac{Signal}{RMS\_noise} = \frac{Light\_in\_pattern - Light\_before\_pattern}{RMS\_noise} \quad (3)$$

The measurement and simulation results shown in Fig. 5 are in excellent agreement with respect to the normalized modulation depth of 70%. Both Figs. 4 and 5 indicate a strong change in the optical evanescent field when the propagating light reaches the adlayer region and past the adlayer, a large damped oscillation of the evanescent field is observed. This oscillation may be caused by the excitation of a second order mode that interferes with the guided first order mode [12]. In this case, leaky higher order mode(s) are excited due to the increase in refractive index near the core that effectively increases the core thickness. The increase in effective core thickness results in a power distribution shift where more of the optical power is contained within the core. If the thickness of the adlayer is large enough, the guiding conditions of the waveguide change such that the propagation of two or more modes becomes possible. Any higher order modes that become excited during the adlayer regions are no longer as tightly bound when the light travels back to the bare waveguide. The transient presence of the higher order mode with the guided mode causes the observed oscillation in the surface evanescent field intensity. The oscillation decays to zero when the power excited into the higher order mode is coupled back into the fundamental mode or is lost from the waveguide. This oscillation impacts the spacing of adjacent capture regions. To obtain an interference free measurement from each capture region, the regions should be spaced such that the light field is able to return to a uniform value. This leaky mode is also observed in the BPM simulation of the light response to the features. It is predicted that a spacing of 200 μm is sufficient for the evanescent field to return to a uniform value.

As may be seen in Figs. 4 and 5, the measured evanescent field intensity at the surface of the sample decreases as the tip is scanned over the region where there is attached photoresist. Two things should be considered when looking at the surface evanescent

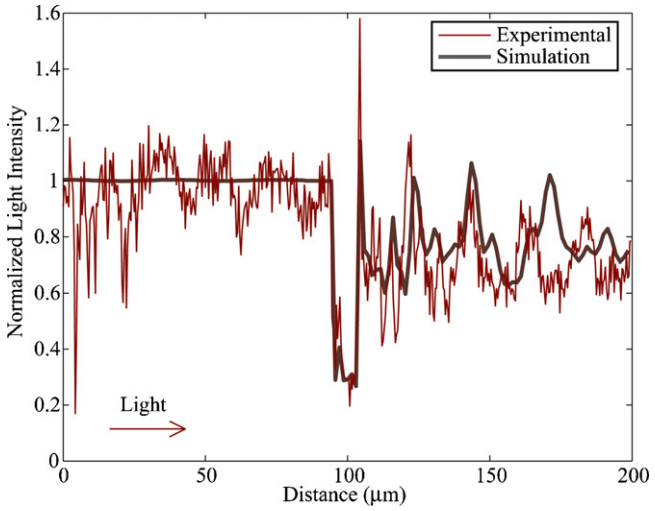

Fig. 5. An overlay of experimental response and simulated response to the 130 nm thick, 8.5 μm long photoresist feature. Light sampled along the top surface of the core and photoresist feature. $\Delta P = 51.9\%$. Light propagates from left to right.

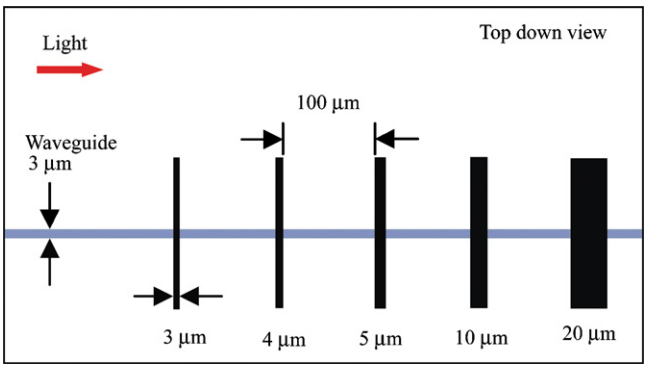

Fig. 6. Mask geometry for fabrication of variable size photoresist features patterned on the waveguide.

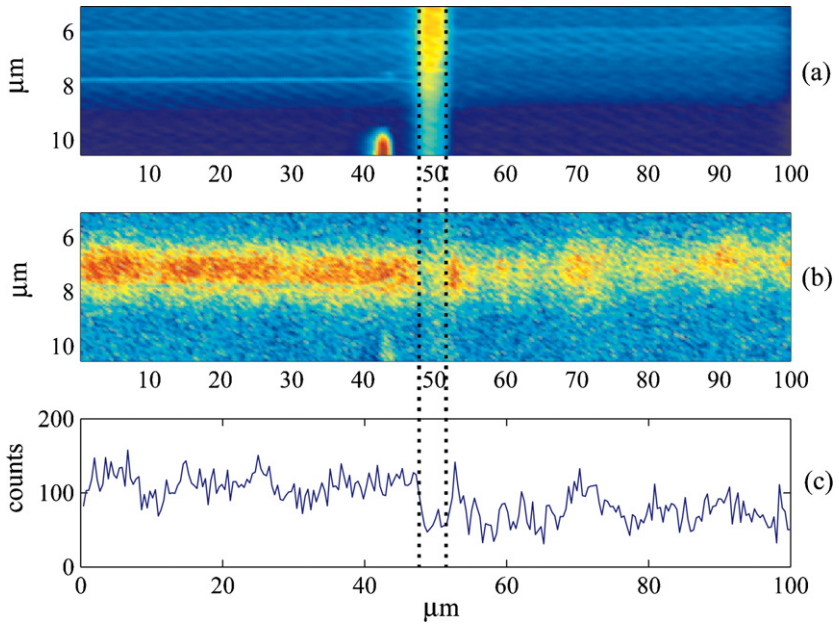

Fig. 7. Light response to small photoresist feature. Light propagates from left to right. (a) Topography of 2.0 μm wide waveguide with 14 nm etch depth. Feature size is ≈3.9 μm in length and 70 nm thick, (b) surface light intensity measured with NSOM, and (c) total light measured in photon counts carried in the waveguide after subtracting the background. $\Delta P = 45.6\%$.

intensity plots generated using NSOM. The evanescent field decays exponentially as the tip is moved away from the surface of the core. Any topographical feature with refractive index lower than the core will produce this effect. This effect occurs for all sizes of topographical features even if the refractive index change is not large enough to cause a shift in the evanescent field. So as the tip scans over a photoresist adlayer, the measured field strength will decrease since the tip moves away from the core/cladding interface. The second effect that occurs is the detection of the shift in the evanescent field as a response to the refractive index change. The presence of the higher refractive index material causes the light to shift up toward the adlayer out of the lower cladding. These two phenomena produce opposite effects on the light intensity measured at the surface. The tip shifting away from the core will reduce the detected signal and the evanescent field shift will increase the detected signal. For surface features near the same refractive index as the core, the effect of the shifting light field is larger than the tip/core distance change and the measured light would tend to increase over adlayer features. In the case of adlayers with refractive index of 1.55, the tip shifting up is the dominant effect on measured light intensity.

To investigate the dependence of signal strength on feature size, a series of adlayers of different lengths were fabricated, shown schematically in Fig. 6, each with a height of approximately 60 nm. The shortest length studied was 2.7 μm. For the 3.9 μm feature seen in Fig. 7, the drop in intensity was followed by an increase and then decaying oscillations indicated that the feature was large enough

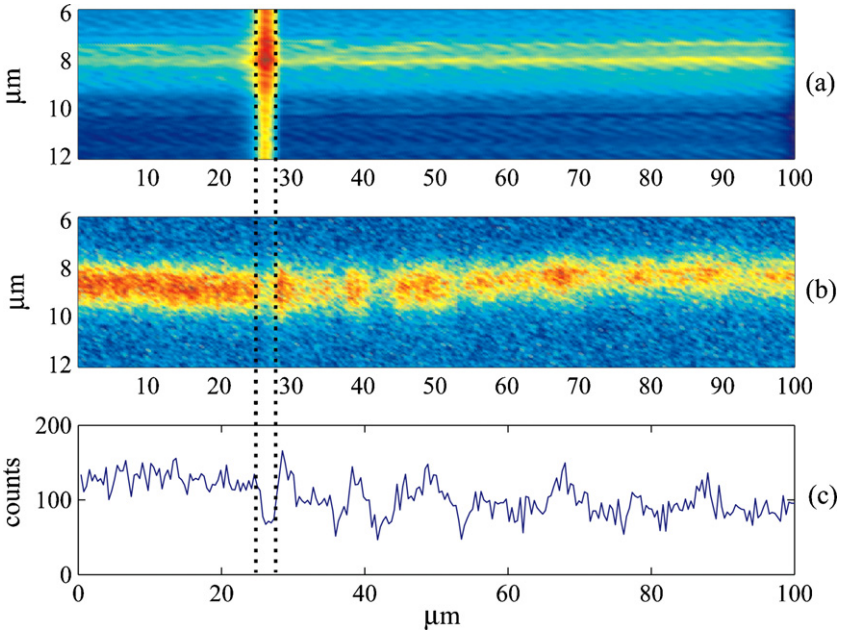

Fig. 8. Light response to the smallest fabricated feature. Light propagates from left to right. (a) Topography of 2.0 μm wide waveguide with 14 nm etch depth. Feature size is ≈2.7 μm in length and 50 nm thick, (b) surface light intensity measured with NSOM, and (c) total light measured in photon counts carried in the waveguide after subtracting the background. $\Delta P = 26.4\%$.

Table 1
Power modulation values and feature sizes for photoresist features shown in the figures.

Feature	Fig. 4	Fig. 5	Fig. 7	Fig. 8
ΔP	76.9%	51.9%	45.6%	26.4%
Feature height	130 nm	130 nm	70 nm	50 nm
Feature length	8.5 μm	8.5 μm	3.9 μm	2.7 μm
S/N	15.9	14.8	3.99	2.79

to cause a change in the evanescent field. A similar response was generated by the 2.7 μm adlayer length, as seen in Fig. 8. The oscillations were definitively present when the 2D light intensity scan was analyzed rather than the total optical power (Fig. 7b). Thus, while it appears there is a minimum length of probe region that is able to generate a significant observable signal, it is shown that 3–4 μm feature sizes still excite a measurable response in the evanescent field. Many current microarray technologies use 20–75 μm diameter spots, which are well over the minimum size that can cause a significant response in the evanescent field. As a next step in the design of the sensor, buried detector elements will be used to measure the evanescent field intensity. The buried detectors will be at a uniform distance from the waveguide core and will not be subject to surface topography effects when measuring the field [16].

4. Conclusion

The evanescent field response in the cases that were studied point toward several conclusions. The presence of the organic material on the surface of the waveguide core excites a weakly bound mode that causes decaying interference with the bound mode. This is a result of the waveguide core dimensions being near the single-mode/multi-mode boundary. Any feature large enough to elicit a response in the evanescent field was also observed to excite a higher order mode over the adlayer region. This result indicates the probe regions be spaced sufficiently far apart to allow for the light field to return to a uniform value. For the system studied here, a spacing of 150–200 μm was enough to allow the oscillation to decay to zero. The evanescent field intensity, measured at the surface of the waveguide/adlayers, decreases as the tip was scanned over the adlayer region and a sharp increase was in evanescent field intensity was observed after the end of the adlayer. The decrease in surface light intensity is due to the photoresist feature having a lower refractive index than the core. The power modulation, due to the presence of the adlayer and the degree of oscillations, increased as the height and length of the adlayer increased as seen in Table 1.

Given the low amount of noise involved in measuring the evanescent field with the NSOM, the apparent minimum length of adlayer that generated a discernable signal was less than the measured 3 μm. The BeamProp simulation results, which contain no adjustable parameters, agree with the measured results and show the same patterns when encountering a photoresist region. These guidelines give insight to design the size and spacing of capture regions in further experimental devices.

Acknowledgements

This work was supported by NIH grant no. EB00726. The authors thank Inverness Medical Professional Diagnostics for the use of their SiN_x deposition equipment.

References

[1] C.A. Rowe-Taitt, J.W. Hazzard, K.E. Hoffman, J.J. Cras, J.P. Golden, F.S. Ligler, Simultaneous detection of six biohazardous agents using a planar waveguide array biosensor, Biosens. Bioelectron. 15 (2000) 579.
[2] F. Ligler, Biosensors for identification of biological warfare agents, Biosens. Bioelectron. 14 (2000) 749.
[3] C.A. Rowe, S.B. Scruggs, M.J. Feldstein, J.P. Golden, F.S. Ligler, An array immunosensor for simultaneous detection of clinical analytes, Anal. Chem. 71 (1999) 433–439.
[4] D.A. Chang-Yen, B.K. Gale, Design, fabrication, and packaging of a practical multianalyte-capable optical biosensor, J. Microlithogr. Microfabr. Microsyst. 5 (2) (2006) 8.
[5] R.M. Ostroff, D. Hopkins, A.B. Haeberli, W. Baouchi, B. Polisky, Thin film biosensor for rapid visual detection of nucleic acid targets, Clin. Chem. (1999) 1644–1659.
[6] C.A.K. Borrebaeck, Antibodies in diagnostics—from immunoassays to protein chips, Immunol. Today 8 (2000).
[7] S.T. Huntington, F. Ladouceur, Evanescent fields—direct measurement, modeling, and application, Microsc. Res. Tech. 70 (3) (2007) 181–183.
[8] T.E. Plowman, S.S. Saavedra, W.M. Reichert, Planar integrated optical methods for examining thin films and their surface adlayers, Biomaterials 19 (1998) 341–355.
[9] R. Bernini, N. Cennamo, A. Minardo, L. Zeni, Planar waveguides for fluorescence-based biosensing: optimization and analysis, IEEE Sens. J. 6 (5) (2006) 1218–1226.
[10] R.G.C. Oudshoorn, R.P.H. Kooyman, J. Greve, Refractive index and layer thickness of an adsorbing protein as reporters of monolayer formation, Thin Solid Films (1996) 284–1284.
[11] G.W. Yuan, M.D. Stephens, D.S. Dandy, K.L. Lear, Novel local evanescent field detection waveguide multianalyte biosensor, SPIE Proc. 5557 (October) (2004) 140–146.
[12] G.W. Yuan, M.D. Stephens, D.S. Dandy, K.L. Lear, Direct imaging of transient interference in a single-mode waveguide using near-field scanning optical microscopy, IEEE Photon. Technol. Lett. 17 (November (11)) (2005) 2382–2384.
[13] J. Benesch, A. Askendal, P. Tengvall, The determination of thickness and surface mass density of mesothick immunoprecipitate layers by null ellipsometry and protein (125)iodine labeling, J. Colloid Interface Sci. 249 (2002) 84–90.
[14] L.S. Jung, C.T. Campbell, T.M. Chinowsky, M.N. Mar, S.S. Yee, Quantitative interpretation of the response of surface plasmon resonance sensors to adsorbed films, Langmuir 14 (1998) 5636–5648.
[15] J. Voros, The density and refractive index of adsorbing protein layers, Biophys. J. 87 (July) (2004) 553–561.
[16] R.J. Yan, S.P. Mestas, G.W. Yuan, R. Safaisini, D.S. Dandy, K.L. Lear, Label-free silicon photonic biosensor system with integrated detector array, Lab Chip 9 (2009) 2163–2168.

Biographies

Matthew Stephens received his BS degree in Chemical Engineering (2002) from Oklahoma State University. He is currently studying for a PhD degree at the Department of Chemical and Biological Engineering, Colorado State University. His current research interests include fabrication and characterization of thin-film waveguides for local evanescent field detection of affinity binding interactions.

Guangwei Yuan received his PhD degree in Electrical Engineering (2008) from Colorado State University. His current interests include numerical simulation of light propagation in slab waveguide structures and circuit design for automated on-chip detection of optical power.

Kevin Lear earned his PhD in Electrical Engineering from Stanford University (1990). After PhD studies as an Office of Naval Research Fellow at Stanford University, Professor Lear joined Sandia National Laboratories as a Senior Member of Technical Staff where he developed high performance laser diode technology. Since moving to Colorado State University his research has focused on photonic biosensors as well as components and systems for high speed optical communication.

David Dandy earned his PhD in Chemical Engineering from the California Institute of Technology (1987). After serving as a senior member of technical staff at Sandia National Laboratories, he joined the faculty at Colorado State University (1992), where his is presently a professor and the head of the Department of Chemical and Biological Engineering. He also has a joint appointment in the School of Biomedical Engineering.